An accessible method for screening aerosol filtration identifies poor-performing commercial masks and respirators

Katherine Schilling Ph.D.,*[,1] Drew R. Gentner Ph.D.,*[,1,2] Lawrence Wilen Ph.D.,*[,3] Antonio Medina,[3] Colby Buehler,[1,2] Luis J. Perez-Lorenzo,[4] Krystal J. Godri Pollitt Ph.D.,[1,5] Reza Bergemann,[3] Nick Bernardo,[3] Jordan Peccia Ph.D.,[1] Vincent Wilczynski Ph.D.,[3] Lisa Lattanza M.D.[6]

[1] Department of Chemical & Environmental Engineering, Yale University, School of Engineering and Applied Science, New Haven, Connecticut 06511, USA

[2] SEARCH (Solutions for Energy, Air, Climate and Health) Center, Yale University, New Haven, CT, USA

[3] School of Engineering and Applied Science, Yale University, New Haven, Connecticut 06511, USA

[4] Department of Mechanical Engineering, Yale University, School of Engineering and Applied Science, New Haven, Connecticut, 06511, USA

[5] Department of Environmental Health Sciences, Yale University, School of Public Health, New Haven, Connecticut, 06510, USA

[6] Department of Orthopaedics and Rehabilitation, Yale University, School of Medicine, New Haven, Connecticut, 06511, USA

*Authors contributed equally to the manuscript

Corresponding author: lisa.lattanza@yale.edu

Abstract

Background

The COVID-19 pandemic has presented an acute shortage of regulation-tested masks. Many of the alternatives available to hospitals have not been certified, leaving uncertainty about their ability to properly protect healthcare workers from SARS-CoV-2 transmission.

Objective

For situations where regulatory methods are not accessible, we present experimental methods to evaluate mask filtration and breathability quickly via cost-effective approaches that could be replicated in communities of need without extensive infrastructure. We demonstrate the need for testing by evaluating an existing diverse inventory of masks/respirators from a local hospital.

Methods

Two experimental approaches are presented to examine both aerosol filtration and flow impedance (i.e. breathability). Mask fit tests were conducted in tandem but are not the focus of this study.

Results

Tests conducted of 47 non-regulation masks reveal variable performance. A number of commercially-available masks in hospital inventories perform similarly to N95 masks for aerosol filtration of 0.2 μm and above, but there is a range of masks with relatively-weaker filtration efficiencies and a subset with poor filtration. All masks functioned acceptably for breathability, and impedance was not correlated with filtration efficiency.

Significance

With simplified tests, organizations with mask/respirator shortages and uncertain inventories can make informed decisions about use and procurement.

Keywords

Personal protective equipment (PPE), masks, N95 respirators, COVID-19, SARS-CoV-2

Introduction

The COVID-19 pandemic has presented an acute need for masks and respirators to be used by healthcare workers on the frontlines and growing needs for essential workers and the public to wear masks in affected areas. The rapid shortage of medical N95 respirators or other certified masks creates an urgent demand for suitable alternatives. This has led to an influx of a wide variety of masks that have not been tested by the National Institute for Occupational Health and Safety (NIOSH) into the medical community and the public with little to no assurance of performance. Hospitals are often faced with deciding which other type of masks (e.g. KN95) to consider buying when the traditional supplies of tested masks are no longer available for purchase. Many claim to have filtration characteristics equivalent to traditional N95 masks but have not undergone the same testing for N95 masks in the U.S. There is also a large influx of counterfeit masks into the market due to mask shortages during the pandemic. Many hospitals are receiving donations from a well-intentioned public that range from non-medical respirators and surgical masks to handsewn facemasks. Most of these donated items have not been confirmed by NIOSH to provide comparable protection from the transmission of SARS-CoV-2 to a standard medical N95 mask (1). As such, the decision to use them without testing information poses significant risk to healthcare and other essential workers.

Currently the number of NIOSH testing facilities in the U.S. are too few to handle the high demand for testing of masks to allow for timely decision making on purchases or the use of donated masks during this critical nationwide shortage. The pandemic and need for accessible mask testing methods are also likely to reach regions with decreased capacity for mask testing (e.g. developing nations). In the absence of available regulation testing facilities or the specific and costly equipment to replicate regulatory methods, we present a screening method to quickly evaluate masks using an accessible approach that could be replicated in communities lacking the infrastructure necessary for regulation tests. These methods are not intended to replace regulation approaches, but to provide alternatives to non-experts in times of need to screen and prioritize the use or acquisition of masks/respirators. As such, readily accessible equipment has been used to maintain accessibility for a greater diversity of communities.

There are several key considerations for mask performance: (a) filtration, (b) flow impedance (i.e. breathability), (c) fit, and (d) continued performance under environmental conditions (e.g. wetting). The assessments performed in this document focuses on the first two aspects. In tandem with this study, masks were also evaluated for fit using a commercial leak detection apparatus, conducted by members of Yale University's Office of Environmental Health and Safety, to characterize and reduce penetration of aerosols at the edges of the masks (2). In order for a mask to be deemed appropriate for clinical use in a COVID-19 patient setting it must pass the filtration and breathability tests as well as a fit test. A variety of methods exist for evaluating the filtration performance of masks/respirators and are summarized and compared in Rengasamy et al. (1), including NIOSH certifications for traditional medical N95 respirators.

Respiratory droplets and aerosols are emitted from humans during coughing, sneezing, breathing, talking, or intubation that could contain viruses, including SARS-CoV-2. Exhaled aerosol/droplets may span from

the nominal size of SARS-CoV-2 (~120 nm) up to 10 μm or larger (3,4,5,6,7,8,9), and can decrease in size with evaporation of condensed water (10,11,12). The World Health Organization identifies two main categories of particles as key factors in coronavirus transmission: "respiratory droplets" (>5 - 10 μm in diameter) and "droplet nuclei" (aerosols <5 μm in diameter) (13); the latter of which includes the typical test aerosol diameters for U.S. agencies involved in mask certification (0.075 - 5 μm) (1). The airborne lifetime of these human-generated aerosol/droplets are size-dependent, reaching upwards of several hours for aerosols in the 0.1 - 1 μm size range (14,15) and suspended SARS-CoV-2 can survive airborne for over 1 hour at moderate humidities (RH = 65%) (16). Aerosols in that size range containing SARS-CoV-2 and surface contamination have been observed in staff areas of hospitals away from patients (8,9,17). Therefore, it is important to consider a wide range of droplet and aerosol sizes for mask filtration efficacy.

Our overall goals are (a) to disseminate simplified testing setups that can be used in comparative evaluations of non-regulation or alternative masks against regulation masks and (b) present results from our survey of a set of commercially-available masks representative of those entering U.S. hospital networks. Testing specifically focuses on flow impedance and aerosol filtration, both of which are evaluated in the traditional NIOSH mask certification process. This study utilizes more readily available equipment and resources to conduct similar assessments in an experimentally-comparable procedure, but does not attempt to replicate or claim NIOSH approval. Its purpose is to allow health professionals to make informed decisions on the most appropriate masks to use when trusted PPE is not available.

Experimental Setup

Filtration Testing Overview

With the intent of evaluating filtration efficiency without purporting to replicate NIOSH equivalency, the methods designed in this study are aimed at testing masks with relevant, reproducible aerosol distributions at face velocities appropriate for human respiration. To evaluate performance, we utilize a combustion-generated polydisperse aerosol and measure removal efficiencies for several size ranges. Using readily-available aerosol instrumentation, size-resolved aerosol number and mass concentrations are measured upstream and downstream of a test mask material. The measured aerosol removal efficiencies of untested respirators and masks are then compared to those of a production lot of regulatory N95 masks to establish performance criteria.

The combustion-generated aerosol is produced via incense inside a sealed 1 m^3 acrylic box that serves as a contained aerosol source (Figure 1). To achieve the desired aerosol concentrations (e.g. 50-100 $\mu g\ m^{-3}$), a stick of burning incense is inserted briefly via a small port in the source chamber. As the incense smolders, it generates humidity and organic compounds, which condense to create a polydisperse aerosol that is geometrically analogous to the respiratory aerosols of concern for coronavirus transmission (see Section S2). Sufficient time is allowed for the aerosol population to become well-mixed and stable in the chamber, using a real-time sensor to track size-resolved concentrations.

The aerosols produced in the source chamber may be too highly concentrated depending on the measurement instrumentation used (e.g. the AirNet aerosol particle counter used in this study). Thus, the flow from the chamber is diluted using pressurized house air that is humidified via a bubbler and regulated by a mass flow controller (AliCat) to control the rate of dilution, though other flow control options are feasible. This diluted aerosol stream is used to test the mask material, which is a disk cut from a full mask using a die for consistency (Figure S3). The disk is housed in a filter holder, in this case a custom aluminum holder with an exposed filter area of 30.5 mm in diameter (Figure S1), but commercially-available filter holders should suffice, and disks may be cut by hand. Grounded metal tubing was used leading to the filter holder and the detectors to reduce losses of charged particles.

However, charge neutralization of aerosols is not employed in this setup, and aerosol charge may play a role in filtration for some masks.

This test method, as with standard test methods, mimics the face velocity (equal to the volume flow rate/surface area) of aerosol deposition on a mask during typical human inspiratory breathing flow rates of 65 - 220 LPM (1) corresponding to face velocities of ~6.4 - 21.7 cm/s for masks ranging in area from 130 - 225 cm^2 (e.g. Table S1). These face velocities are achieved with our 30.5mm disk sample using volume flow rates from 2.8 - 9.5 LPM and most of the testing focused on 4.5 LPM corresponding to 10 cm/s.

Two real-time detectors were used in the study, an AirNet (model 210, Particle Measurement Systems) and a SEARCH multipollutant monitor equipped with a Plantower A003 sensor from the "Solutions for Energy, AiR, Climate, and Health" Center at Yale-Johns Hopkins (18). Other detectors may be used, provided the careful considerations detailed in this paper are followed. The AirNet detector measures the number concentration of aerosols in size bins of 0.2 - 0.3 µm, 0.3 - 0.5 µm, 0.5 - 1 µm, and >1 µm. The SEARCH monitor measures mass and number concentrations of aerosols in size bins 0.3 - 0.5 µm, 0.5 - 1 µm, 1 - 2.5 µm, 2.5 - 5 µm, and 2.5 - 10 µm with a lower sensitivity compared to the AirNet (18).

Upstream of the filter, the SEARCH detector is used to monitor and maintain reproducible and stable test aerosol concentrations in the source chamber. Downstream of the filter, aerosol concentrations were measured with both the AirNet and a second SEARCH instrument for redundancy. However, the analysis was done primarily with the AirNet to demonstrate that only a single reliable detector is critical for such an assessment. Downstream concentrations of the aerosols are checked regularly without a mask in place to confirm that they match those expected based on the source chamber concentrations and dilution rates. Periodic downstream measurements with the second SEARCH monitor were done to cross-check the observed filtration efficiencies, dilution rates, and aerosol transmission.

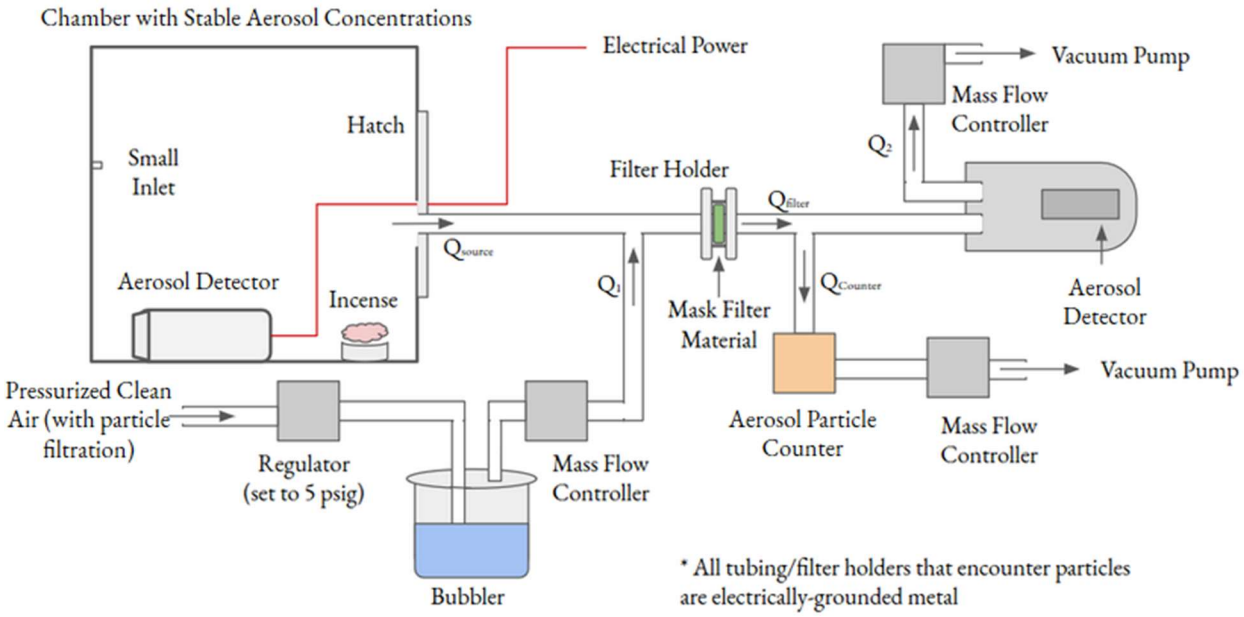

Figure 1: Primary experimental setup for aerosol filtration assessment, where the "aerosol detectors" refer to SEARCH monitors and the "aerosol particle counter" is the AirNet instrument (in orange).

Downstream flow rates are controlled to change the face velocity used to test the filter material and provide the suction from the source chamber. The AirNet is controlled by a built-in orifice (2.8 LPM) and

a second mass flow controller (AliCat) is used to pull the remainder of the flow through the system (e.g. 1.7 SPLM for a 10 cm/s face velocity), where vacuum is generated using 2 separate vacuum pumps. At any given face velocity, changing the dilution flow rate adjusts the test aerosol concentration. A more detailed description of the flow rates shown in Figure 1 can be found in Section S1. The filtration efficiency for any of the size-resolved bins is defined as:

Filtration Efficiency [%] = $(1- C_{downstream}/C_{upstream}) \times 100\%$

and for the purposes of this study was further substantiated by measuring across a series of dilution factors (with and without mask material in place) to gain multi-point measurements across a range of test aerosol concentrations at a given face velocity (see Section S4 & Figure S6).

Flow Impedance Testing

Flow impedance assessment of the mask materials is conducted to gauge the potential breathability of a given mask. Proper use of a mask mandates that the mask creates a good seal around one's face. This forces intake air to be limited to what can pass easily through the mask, which means that enough pressure is needed from breathing to drive the air flow. Regardless of filtration capability, a mask with low breathability still poses a risk to the wearer due to the difficulty of breathing normally.

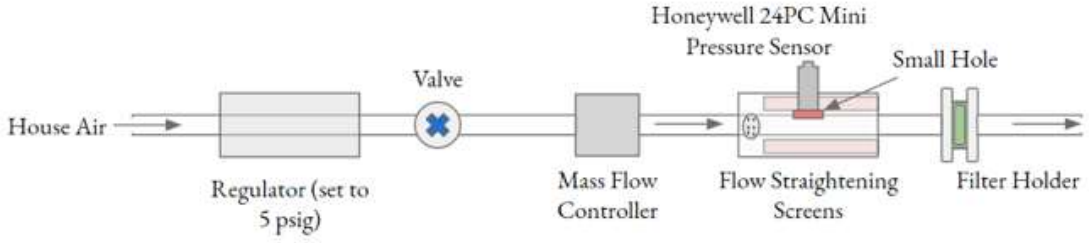

Figure 2: Experimental setup to test flow impedance test for breathability (19).

The NIOSH procedure takes into account the effect of mask area on the maximum pressure allowed for a specified volume flow (the ratio defining an "extrinsic impedance") by using a full mask for the test. Here, we employed a straightforward apparatus to measure the *intrinsic* impedance of mask material by measuring the pressure drop (in mm H_2O) across a 40 mm disk of mask filter material as a function of the face velocity (calculated from the volume flow rate and the 40 mm disk area of 12.6 cm^2). The slope of the linear fit to these points is the intrinsic impedance of the material in units of mm H_2O / (cm/s). The experimental apparatus (Figure 2) is from Petculescu & Wilen (19) and further described in Section S3.

To get a value for the extrinsic impedance for a given mask, we divide the intrinsic impedance by the mask area, either measured directly or approximated based on mask type and geometry. It should be noted that the instrumentation used here could easily be replaced with low cost commercial rotameters and manometers to measure flow and pressure.

A rapid screening setup for testing aerosol filtration

We also evaluated a rapid screening approach with the understanding that initial screening of large inventories is necessary to determine which masks/respirators warrant further testing and also that some communities and facilities may be constrained in terms of available instrumentation for aerosol measurement and flow control. This further-simplified setup (Figure 3) relies on a filter holder (well-sealed) and a single AirNet 210 detector, with a fixed volume flow rate of 2.8 LPM, and configured to

read out count data through its analog outputs. A commercially-available, plastic filter holder was intentionally used and the face velocity through the filter was modified with a pair of laser-cut ring inserts to test at 10 cm/s (see images in Figure S2). With this setup, adjusting the filter area to achieve the appropriate face velocity is critical, otherwise slow face velocities atypical of breathing conditions might skew results and give false positive results.

An example procedure is shown in Figure 3B where two mask materials are inserted and removed to assess against upstream concentrations without the mask in place. If ambient aerosol concentrations are sufficiently stable in the room where testing is occurring, ambient air can serve as the aerosol "source", as was the case for this evaluation approach. Data and results of this testing are described in supplemental information. Although a second AirNet 210 detector was used here, which allowed for a direct comparison to the full technique, any instrument that provides size-resolved aerosol concentration measurements could possibly work for this approach (see *Considerations* section).

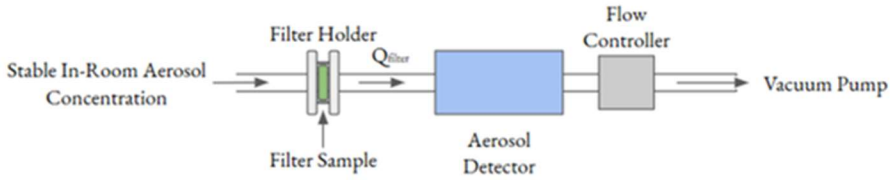

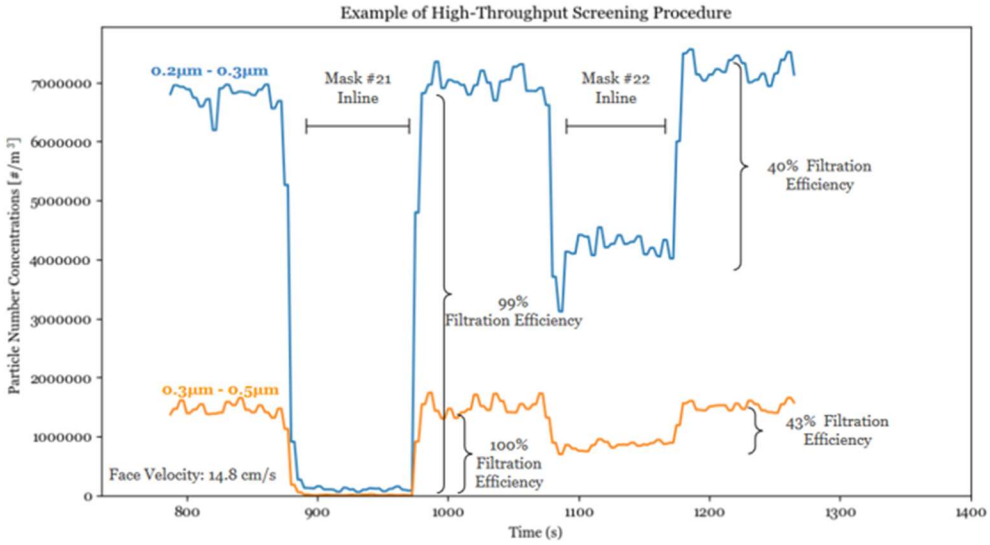

Figure 3: A rapid screening setup with (A) schematic and (B) example test procedure.

Results & Discussion

Aerosol Filtration Efficiency

While the instrumentation package measured an aerosol size range of 0.2 - 10 µm, aerosol filtration analysis focused on the range of 0.2 - 1 µm for these reasons: this range is closer to sizes of interest in the NIOSH/FDA methods; it targets the most challenging aerosols to filter (0.2 - 0.3 µm); and this particle diameter range is where mask performance differentiated most for the masks and instruments used in this study. A set of face velocities were examined to span typical inspiratory flow rates and typical test

procedures (1), but primarily focused on 10 cm/s for inventory screening (Figure 4) as discussed earlier. Prior to recommending that a mask be used in service, multiple trials of the same mask type across a set of individual masks from a delivered lot are conducted to ensure consistent results in the data. Results from repeated tests of a single mask type (Figures 4A inset) show variability within mask lots, which were larger for a poorly-performing mask type (#15), compared to the six N95 tests that ranged 98-99% at 10 cm/s. Repeat tests of the same exact mask sample on different days resulted in minimal variance and demonstrated consistency in the experimental setup. Specifically, the error was 0.7 ± 0.6 % in absolute deviation between tests (i.e. $Eff._{test\ t}$ -$Eff._{test\ t+1}$) for the 0.2 - 0.3 µm size bin.

As shown in Figure 4, tests conducted on 47 non-regulation masks using this setup reveal that a number of commercially-available masks perform similarly to the regulation N95 mask's aerosol filtration for 0.2 µm and above. Then, there are a range of masks with relatively weaker filtration efficiencies (i.e. 80% - 95% for aerosols >0.2 µm). Yet, a subset of commercially-available masks have poor performance (i.e. <80%) relative to N95 or similar masks. It is important to note that the masks tested here focus on non-regulated, commercially-available masks., most of which are purported to be efficacious for aerosol filtration at, or near, that of an N95 respirator (Table S1). The performance of the ten commercial (traditional) surgical-style masks tested varied widely 22 - 95% (see Table S1) with an average of 72 ± 19%. While materials for homemade masks could be tested with this setup, it was generally outside the scope of this PPE survey (the 1 homemade mask and 1 commercially-made alternative mask donated to the hospital included in this study performed very poorly, i.e. 14%).

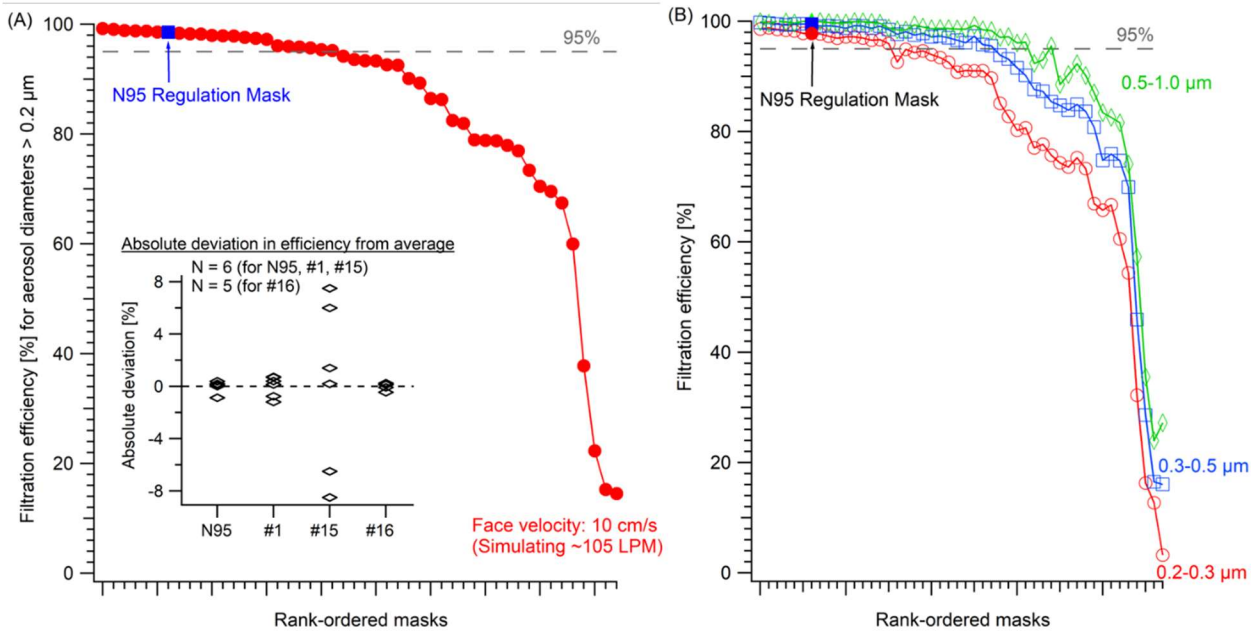

Figure 4: Filtration efficiency of 47 commercially-available masks for (A) all aerosols of 0.2 µm and larger, shown with a regulation-tested N95 mask (blue marker) at a face velocity of 10 cm/s, roughly simulating an 105 LPM inspiratory breathing rate; and (B) mask performance shown for three aerosol size fractions from 0.2 to 1 µm. Efficiencies shown are determined via aerosol number concentrations and the Panel A inset shows variations across masks tested for 4 mask types, displayed as the absolute deviation in aerosol filtration efficiency from the average (i.e. $Eff._{Sample\ i}$ - $Eff._{Avg.}$). Note: mask numbers in the inset (and Figure 5) refer to cataloging in Table S1 and not rank-ordered performance.

There was significant disparity in the performance of masks purported to be N95 equivalent (i.e. KN95) or even labeled as "N95", spanning efficiencies of 38% (Mask #22) to 99% (see Table S1 for values). Some KN95 masks performed consistently well, but others did not. For example, Mask #1 performed consistently well while Mask #15 had significant variance (Figure 4A inset) with 2 masks from #15's lot performing at or near 95% filtration and others reaching as low as 78-82%. These results raise the importance of both testing a significant sample size of masks from any received lots and the value of validation independent of vendor assurances.

Mask filtration efficiencies expectedly varied as a function of aerosol size. Given the higher efficiency of inertial impaction for larger aerosols with more mass and momentum, the masks generally performed better for larger aerosols (Figure 5). While mask filtration performance can be similarly differentiated, absolute efficiencies are greater when considering all aerosols (i.e. >0.2 μm) than solely aerosols of 0.2 - 0.3 μm (Figures 4, S7). Consistent with aerosol filtration theory, the removal of smaller aerosols is better at slower face velocities (Figure 5) given the dependence of "diffusive" losses (i.e. Brownian motion to the filter fibers) on flow rates (i.e. timescales for air transport through the filters). This aerosol size dependence is important since SARS-CoV-2-containing aerosols are distributed across a wide size range and aerosols with diameters of 0.1-0.5 μm can remain airborne longer (8,9,14,15). With regard to testing protocols, Figure 5 demonstrates clearly how flow rate (i.e. face velocity) influences filtration efficiencies.

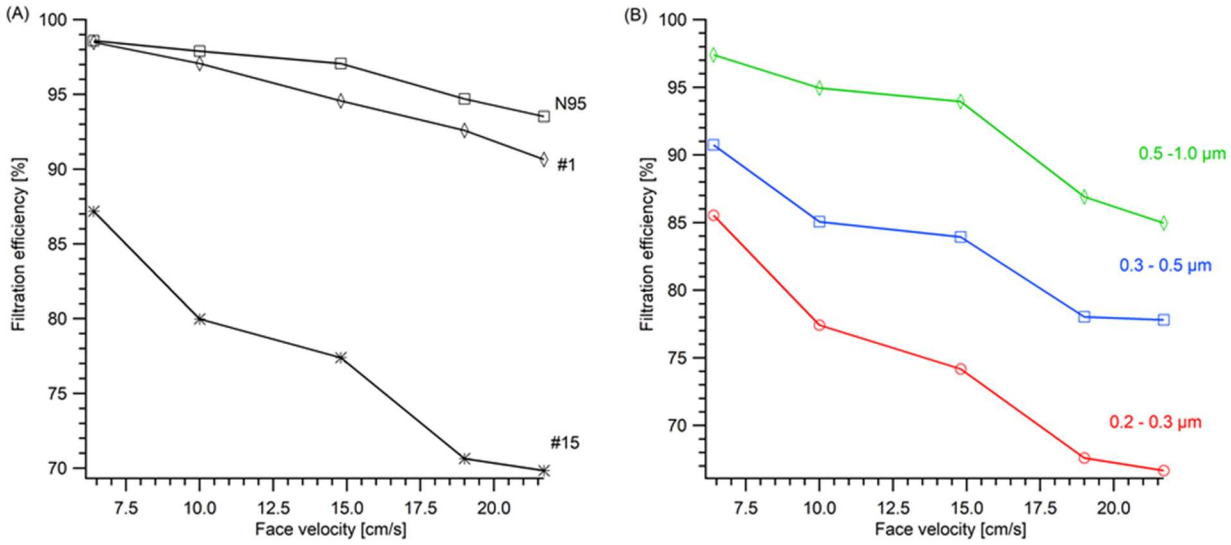

Figure 5: Filtration efficiency as a function of face velocity resulting from typical breathing flow rates. (A) Aerosol removal efficiency (>0.2 μm) of 3 masks: an N95 regulation mask and 2 masks marketed as KN95 (#1 & #15). (B) Size-resolved removal efficiency for a moderately-performing mask (#15 from Panel A).

Impedance and Breathability

Using the technique described above, the intrinsic impedance was measured and tabulated for the mask inventory (Figure 6). The extrinsic impedance was also examined for some of the masks for which areas had been measured independently using an image analysis technique (see SI). All the extrinsic impedances are below the NIOSH threshold (Table S1), and even for masks for which areas were not measured, based on their intrinsic impedances, their areas would have to be improbably small to exceed the NIOSH threshold for breathability. For simplicity in comparison, we also present an "intrinsic

breathability index" which is defined as the ratio of the intrinsic impedance for a mask compared to a standard N95 mask. In Section S4, we discuss various implications for the filtration, impedance, and face sealing relating to the mask area. Presented with a large array of masks to test, efforts to include area measurement were streamlined. Some masks were excluded from consideration early, based on poor filtration of the mask material. Masks found to be made of material with the highest measured filtration efficiencies were prioritized for more extensive examination. Among these, higher priority for use in hospitals was then given to masks with the smallest extrinsic impedance, also taking face sealing into account.

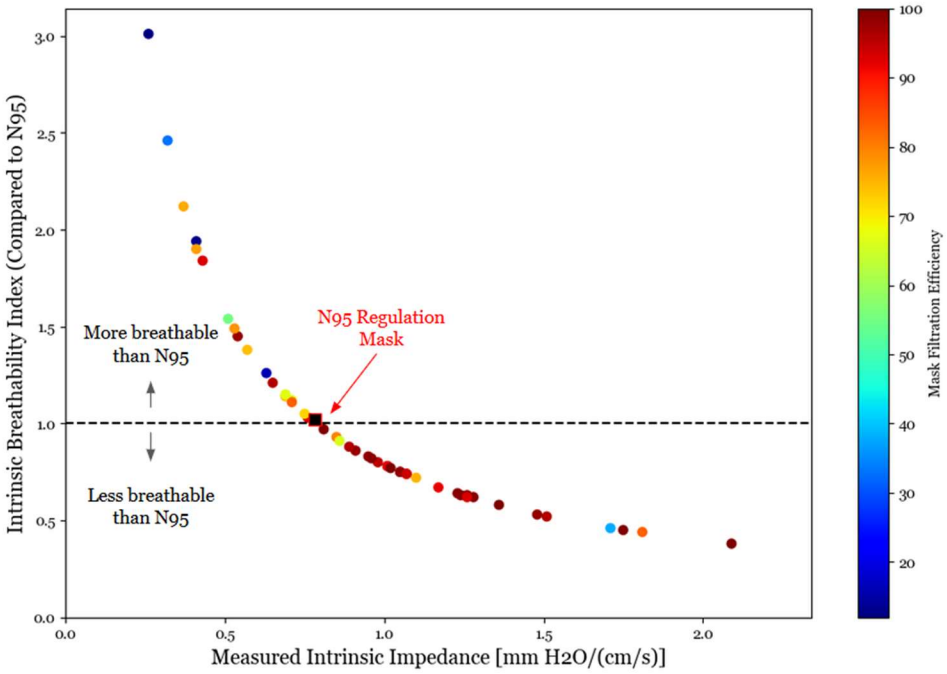

Figure 6: Measured impedance values shown against breathability index (i.e. N95 intrinsic impedance / intrinsic impedance) where all masks are within the NIOSH threshold for impedance. Points are colored based on filtration efficiency, and no correlation was observed between impedance and filtration efficiency.

Rapid Screening Results

To evaluate the rapid screening setup (Figure 3), we tested this approach for half of the masks tested in the Figure 1 setup. The rapid screening approach's filtration efficiencies were consistent with those of the primary setup and effective for rank-ordering masks (Figure 7). The differences in filtration efficiencies in Figure 7 are not random, but well-correlated when fit to a power function (Figure S13), potentially owing to the combined effects of differences in in-room aerosol size distributions and face velocities. Based on these results, we conclude that this method has efficacy as a rapid screening method, where 26 masks can be preliminarily screened in 80 minutes (Figure S11). However, frequent cross-comparison to N95 benchmark masks is essential between operational sessions since variations in-room aerosol composition can affect results. More details about correlations between the two techniques and calibration procedures are described in the Section S5.

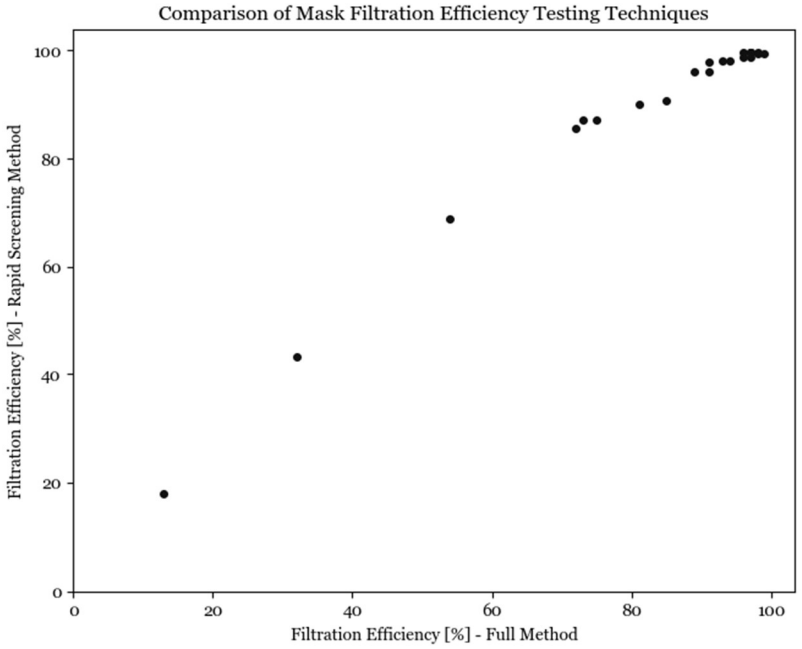

Figure 7: Comparison of rapid screening setup (Figure 3) compared to primary setup (Figure 1) showing equivalent ranking of mask/respirator performance. Filtration efficiencies are shown for 0.2 - 0.3 μm aerosols. Note: Tested face velocities were not the same between the 2 approaches.

Conclusions: Considerations & Best Practices

As defined above, these methods are not intended to replace regulation approaches, but to provide accessible screening approaches where necessary for emergency evaluation of incoming masks/respirators. The goal is to allow users to rank-order masks in comparison to N95 "benchmark" masks (in their possession) to enable more informed decisions and prioritization of PPE for use. Mask fit and durability must also be assessed. To facilitate replicate setups, we outline a selection of considerations, potential issues, and best practices with additional detail in Section S4. Given that all masks here performed sufficiently in terms of breathability (i.e. flow impedance) compared to the NIOSH threshold, our discussion in the main text is focused on filtration test considerations, where the tested masks performed more variably.

The primary testing setup described in Figure 1 is not the sole feasible configuration, as is readily demonstrated with the rapid screening approach (Figure 3). However, the primary setup does offer certain advantages that should be considered by future users: (a) consistent and stable spherical polydisperse aerosol populations that span the range of target aerosol sizes; (b) repeatable flow rates delivering the test aerosol mixture at atmospheric pressure and representative face velocities (e.g. 10 cm/s) that allow for discrimination of mask performance; (c) leak-checked systems, especially in the filter holder where bulky mask materials increase the potential for leaks (note: flow balance can be confirmed using multiple flow controllers; Figure 1); (d) frequent confirmation of test aerosol concentrations via downstream instruments (with no filter in place) checked at all flow and dilution conditions used, with redundant instruments up- and down-stream (if available); (e) regular checks of filtration efficiency against N95 "benchmark" masks; and (f) metal tubing and filter holder (all grounded) are best practice to avoid electrostatic aerosol losses, but non-metallic components may work with frequent comparisons to "blank"

measurements without a filter. Similarly, digital mass flow controllers are used in this study, but sufficiently precise rotameters or flow constrictions may prove effective substitutes.

Aerosol instrumentation is a critical consideration, and differences between available instrumentation are considerable across the global scientific and hospital community. As such, this study is carried out using a total aerosol instrumentation cost of under $2000 USD, and found high utility in the AirNet aerosol particle counter used for clean-room monitoring. While multiple monitors are included in Figure 1 and used in cross-checks, the conclusions were derived primarily with a single detector. The key elements are that (a) the aerosol concentrations used for testing must be adjusted based on the sensitivity of the instrumentation such that the signal-to-noise ratio of the measurements are sufficiently high to determine the filtration efficiency with some precision (i.e. accurately measure changes between upstream and downstream concentrations) while also avoiding exceeding upper limits of detection or linearity; (b) real-time instruments allow for faster screening of inventories and prioritization of masks; (c) size-resolved measurements are better suited to discern differences in mask performance and more closely match aerosols in NIOSH/FDA tests since larger, easily-filtered aerosols are major contributors to the mass distributions of combustion or in-room aerosols; and (d) it is beneficial to use aerosols that span the range of sizes of potentially virus-containing aerosols (>0.2 μm in this setup), but smaller aerosols in this range are more challenging to filter at the typical face velocities and are preferentially tested in the NIOSH and FDA procedures. Yet, total aerosol number concentration measurements without size-resolution that include sizes below 0.1 μm may skew efficiency results by incorporating filtration of combustion or in-room aerosols dominated by these smaller sizes, which are easily collected via Brownian motion, and are outside the size range of interest for SARS-CoV-2 aerosol transmission. While aerosol number concentrations were used to determine filtration efficiencies in this study, size-resolved mass concentrations could be used with appropriate test aerosol concentrations and instrument sensitivities.

Regardless of the testing setup, it is essential to screen a sufficient number of masks/respirators to constrain lot-to-lot variability (e.g. Figure 4A inset) for masks that might be used in service. The NIOSH protocol requires 20 of 20 masks to exceed the 95% filtration efficiency. The exact number of randomly-selected masks to be tested by an organization may depend on the supply of masks in a given lot and their likely application, but based on our results there are clear indicators of mask-to-mask variance within a sample size of 5 masks (Figure 4A inset) that could be used to inform further examinations of variance.

Given that aerosol filtration efficiency varies with aerosol size, larger aerosols will be removed more effectively (i.e. 1-5 μm), but smaller aerosols (e.g. 0.2-0.5 μm) may provide more ability to discern between mask/respirator performance. Similarly, faster flow rates may provide more potential to discern between masks, yet care should be taken to not extend velocities outside the range of the typical conditions during breathing (coughing, speaking, etc.) that are examined in regulation testing (e.g. 3-14 cm/s) (1). For a given flow rate, differences in face velocity with a full mask, compared to the subsections tested here, will vary with mask area, such that a larger surface area mask will have lower face velocities while in-use. Yet changes in filtration efficiencies for well-performing masks will be minor (e.g. with a decrease from 10 cm/s to 7.5 cm/s; Figure 5A) and the face velocity can be adjusted to account for the mask area where necessary for verification.

The methods presented here rely upon regular comparisons to NIOSH N95 benchmark masks, as absolute filtration efficiencies will vary with changes in flow rates and aerosol sizes measured (e.g. Figure 5). Similar aerosol concentrations and consistent flow conditions between masks must be maintained to minimize system variance that could affect data interpretation. Validation of a system should include

testing a range of materials expected to have both excellent and poor filtration efficiencies. Finally, this approach does not convey the equivalent of an N95 certification, and this publication does not include a full comparison to NIOSH results other than the comparison to available N95-compliant masks.

Acknowledgements: We would like to thank Dan Rosner, Jenna Ditto, and Juan de la Mora (Yale) for loaning equipment/instrumentation and/or helpful discussions. The SEARCH monitor used in this study was developed under Assistance Agreement No. RD835871 awarded by the U.S. Environmental Protection Agency to Yale University. It has not been formally reviewed by EPA. The views expressed in this document are solely those of the authors and do not necessarily reflect those of the Agency. EPA does not endorse any products or commercial services mentioned in this publication. C.B. is supported by the National Science Foundation Graduate Research Fellowship Program under Grant No. DGE1752134. Any opinions, findings, and conclusions or recommendations expressed in this material are those of the author(s) and do not necessarily reflect the views of the National Science Foundation.

Conflict of interests: D.R.G. has externally-funded projects on low-cost air quality monitoring technology (EPA, HKF Technology), which Yale has licensed to HKF Technology.

References

1. Rengasamy S, Shaffer R, Williams B, Smit S. A comparison of facemask and respirator filtration test methods. Journal of occupational and environmental hygiene. 2017 Feb 1;14(2):92-103.
2. The National Institute for Occupational Health and Safety. "Filtering out Confusion: Frequently Asked Questions about Respiratory Protection, Fit Testing", Publication No. 2018-129, 2018. doi:10.26616/NIOSHPUB2018129 https://www.cdc.gov/niosh/docs/2018-129/pdfs/2018-129.pdf?id=10.26616/NIOSHPUB2018129
3. Lindsley WG, Pearce TA, Hudnall JB, Davis KA, Davis SM, Fisher MA, Khakoo R, Palmer JE, Clark KE, Celik I, Coffey CC. Quantity and size distribution of cough-generated aerosol particles produced by influenza patients during and after illness. Journal of occupational and environmental hygiene. 2012 Jul 1;9(7):443-9.
4. Milton DK, Fabian MP, Cowling BJ, Grantham ML, McDevitt JJ. Influenza virus aerosols in human exhaled breath: particle size, culturability, and effect of surgical masks. PLoS pathogens. 2013 Mar;9(3).
5. Morawska LJ, Johnson GR, Ristovski ZD, Hargreaves M, Mengersen K, Corbett S, Chao CY, Li Y, Katoshevski D. Size distribution and sites of origin of droplets expelled from the human respiratory tract during expiratory activities. Journal of Aerosol Science. 2009 Mar 1;40(3):256-69.
6. Papineni RS, Rosenthal FS. The size distribution of droplets in the exhaled breath of healthy human subjects. Journal of Aerosol Medicine. 1997;10(2):105-16.
7. Xie X, Li Y, Sun H, Liu L. Exhaled droplets due to talking and coughing. Journal of the Royal Society Interface. 2009 Dec 6;6(suppl_6):S703-14.
8. Liu Y, Ning Z, Chen Y, Guo M, Liu Y, Gali NK, Sun L, Duan Y, Cai J, Westerdahl D, Liu X. Aerodynamic characteristics and RNA concentration of SARS-CoV-2 aerosol in Wuhan hospitals during COVID-19 outbreak. bioRxiv. 2020 Jan 1.
9. Chia PY, Coleman KK, Tan YK, Ong SW, Gum M, Lau SK, Sutjipto S, Lee PH, Young BE, Milton DK, Gray GC. Detection of Air and Surface Contamination by Severe Acute Respiratory

Syndrome Coronavirus 2 (SARS-CoV-2) in Hospital Rooms of Infected Patients. medRxiv. 2020 Jan 1.

10. Mikhailov E, Vlasenko S, Niessner R, Pöschl U. Interaction of aerosol particles composed of protein and salts with water vapor: hygroscopic growth and microstructural rearrangement. 2004.
11. Yang W, Marr LC. Dynamics of airborne influenza A viruses indoors and dependence on humidity. PloS one. 2011;6(6).
12. Goldsmith CS, Tatti KM, Ksiazek TG, Rollin PE, Comer JA, Lee WW, Rota PA, Bankamp B, Bellini WJ, Zaki SR. Ultrastructural characterization of SARS coronavirus. Emerging infectious diseases. 2004 Feb;10(2):320.
13. World Health Organization. Modes of transmission of virus causing COVID-19: implications for IPC precaution recommendations: scientific brief, 27 March 2020. World Health Organization; 2020.
14. Nazaroff, W.W., Indoor particle dynamics. 2004.
15. Lai AC, Nazaroff WW. Modeling indoor particle deposition from turbulent flow onto smooth surfaces. Journal of aerosol science. 2000 Apr 1;31(4):463-76.
16. van Doremalen N, Bushmaker T, Morris DH, Holbrook MG, Gamble A, Williamson BN, Tamin A, Harcourt JL, Thornburg NJ, Gerber SI, Lloyd-Smith JO. Aerosol and surface stability of SARS-CoV-2 as compared with SARS-CoV-1. New England Journal of Medicine. 2020 Mar 17.
17. Santarpia JL, Rivera DN, Herrera V, Morwitzer MJ, Creager H, Santarpia GW, Crown KK, Brett-Major D, Schnaubelt E, Broadhurst MJ, Lawler JV. Transmission potential of SARS-CoV-2 in viral shedding observed at the University of Nebraska Medical Center. medRxiv. 2020 Jan 1.
18. Levy Zamora M, Xiong F, Gentner D, Kerkez B, Kohrman-Glaser J, Koehler K. Field and laboratory evaluations of the low-cost plantower particulate matter sensor. Environmental science & technology. 2018 Dec 18;53(2):838-49.
19. Petculescu A, Wilen LA. Oscillatory flow in jet pumps: Nonlinear effects and minor losses. The Journal of the Acoustical Society of America. 2003 Mar;113(3):1282-92.
20. Jetter JJ, Guo Z, McBrian JA, Flynn MR. Characterization of emissions from burning incense. Science of the Total Environment. 2002 Aug 5;295(1-3):51-67.
21. Wang B, Lee SC, Ho KF. Chemical composition of fine particles from incense burning in a large environmental chamber. Atmospheric environment. 2006 Dec 1;40(40):7858-68.
22. Lin TC, Krishnaswamy G, Chi DS. Incense smoke: clinical, structural and molecular effects on airway disease. Clinical and Molecular Allergy. 2008 Dec 1;6(1):3.

Supplemental Information

Section S1: Flow definitions and information (see Figure 1).

- Flow from MFC 1 was defined to be Q1 (i.e. dilution air)
- Flow from MFC 2 was defined to be Q2
- Flow through AirNet detector was controlled to be 2.8 SLPM with a third MFC
- Q_filter = Q2 + 2.8
- Q_source = Q_filter – Q1
- Balance point is defined to be when Q_source = 0 which is when Q1 = Q2 + 2.8
- Q_source can also be set negative to get a definitive zero for aerosols flowing to filter, but can also be used to dilute the aerosol concentration in the source chamber
- House air was regulated to 5 psig and run through a bubbler made from a water squeeze bottle as the input to MFC1
- A vacuum pump was the outlet to MFC2
- A separate vacuum pump was the outlet to the MFC on the downstream side of the AirNet detector
- Flow through the filter (Q_filter) was typically controlled to be either 4.5 SLPM, corresponding to face velocities of 10.3 cm/s
- Flow coming from the source chamber (Q_source) was independently controlled using combination of flow controllers (AliCat)
- Dilution factor (DF) of aerosol source was defined to be Q_source/Q_filter

Section S2: Use of incense as a polydisperse aerosol source

For the purposes of mask screening and prioritization, this approach assumes that the on-mask mechanisms of collection of these spherical organic aerosols can be used as a proxy to respiratory aerosols or the NaCl or latex particles used in regulation tests. Although incense is not historically used to evaluate mask effectiveness, there are several reasons this study uses incense as an aerosol source. Incense burning generates a polydisperse aerosol that has some water present from the combustion process (20,21,22), and humidity is actively maintained in the dilution setup to prevent aerosols from drying out. The aerosol size distribution from incense combustion spans the sizes of interest (20,21,22), from the diameter of SARS-CoV-2 itself up to droplets produced from the respiratory system (e.g. coughing, sneezing, breathing, talking), ranging from under 100 nm to 10 μm. Furthermore, it is easily-attainable globally, making it a desirable aerosol source for mask filtration assessment.

Among combustion sources, incense typically has a high organic carbon to elemental carbon ratio (22 on average), which means that the aerosols produced from smoldering will be predominantly spherical organic carbon, not elemental carbon soot chains, with a density similar to water (1 g/cm^3) (21). This is an important consideration because it ensures that the particle shapes used in testing are similar to spherical human-generated aerosols and optical measurements of aerosol size will be similar to the aerodynamic diameter that influences the mechanisms of deposition onto filters/masks. The combustion-based aerosol source brings the added benefit of being relatively easy to generate/maintain a reproducible, persistent

polydisperse aerosol concentration that can stabilize in an isolated chamber; these factors allow for multiple tests to be run sequentially. Using a combustion-based aerosol source circumvents the need to obtain and operate a nebulizer, atomizer, differential mobility analyzer, or other equipment for standardized aerosol generation, with the benefit that there is less concern about aerosol evaporation. Furthermore, the instruments used here are designed to make accurate measurements of combustion-related aerosols common in outdoor pollution similar to those generated from incense, as opposed to highly reflective aerosols (e.g. NaCl) that could pose problems for some low-cost light scattering-based instrumentation (18).

One important consideration for using this approach is that sufficient time must be allowed for concentrations to stabilize in the chamber, providing a well-mixed test aerosol. Two approaches we tested to achieve elevated aerosol concentrations in the chamber: a stick of burning incense is inserted briefly via a small port in the source chamber, or a small amount of incense is placed into an aluminum foil bowl, where it is lit and allowed to smolder in the chamber until it burns out. However, the first method was primarily used as it was found to be more efficient.

Based on the in-chamber measurements (with the SEARCH monitor), aerosols smaller than 1 μm represented approximately half or more of the aerosol mass concentrations, and aerosol number concentrations were distributed across the size bins (e.g. 61% in 0.2-0.3 μm, 31% in 0.3-0.5 μm, and 7% in 0.5-1 μm, prior to any correction for counting efficiencies in AirNet monitor).

Section S3: Additional details on impedance measurements

For a given mask, this flow impedance of a mask is determined by the pressure required to achieve a specified volume flow through the mask. NIOSH Procedure No. TEB-APR-STP-0007 specifies that "for non-powered, air-purifying particulate respirators upon initial inhalation shall not exceed 35 mm water-column." The procedure calls for a test volume flow rate of 85 LPM. The pressure divided by the volumetric flow rate is an extrinsic measure of the mask impedance with units of mm H_2O / (cm^3/s) (where 1 LPM = 1000 cm^3 / 60s = 16.67 cm^3/s). The test therefore specifies a maximum extrinsic impedance of 0.0247 mm H_2O / (cm^3/s).

The experimental setup shown in Figure 2 is the same as described in Petculescu & Wilen (19). A Matheson flow controller connected to the house air regulated to 5 psig defines the volume flow rate in the system. The pressure is measured just upstream of the filter holder in an aluminum tube of inner diameter 15.8 mm, which leads into the filter holder connection. The flow into the tube is conditioned with screens to improve laminarity and reduce any possible fluctuations due to turbulence from changes in cross section. A hole leads from the pressure gauge to the inside of the tube. Inside the tube the hole is covered with aluminum foil tape, but a pinhole in the tape allows pressure equilibration to the gauge, which measures the pressure inside the tube with respect to atmospheric pressure. The pressure gauge is a Honeywell Microswitch PC24 sensor, based on a standard Wheatstone bridge strain gauge. The bridge was excited with 5 VDC and read out with a Keithley 2000 multimeter. The signal was calibrated against an analog manometer with a full-scale pressure of 25.4 mm H_2O. We determined a calibration of 26.7 μV/ mm H_2O.

In order to make an accurate measurement of the filter impedance, it is necessary to account for pressure drops that may result from the filter holder and the connections leading into and out of it.

We were careful to measure the pressure drop across the filter alone by first measuring the flow curve for the empty filter holder, and then measuring the flow curve for the filter holder with the filter sample in place. Subtraction then yields a flow curve for the sample alone. Figure S8 shows the three curves for one sample. The slope of the difference curve yields the intrinsic impedance. Such flow curves were observed to be very linear in all cases. For any data shown henceforth, flow curves with the subtraction for the filter holder has been performed.

A number of checks were performed to confirm measurement repeatability. Two samples in series (i.e. stacked in the filter holder) should yield an impedance that is the sum of the impedances for each sample measured alone. Figure S9 with the flow curves demonstrates this consistency (with the filter holder subtraction discussed above already performed). A second test for consistency is to show that the flow curve for pressure versus face velocity does not depend on the sample area. We used pairs of machined aluminum rings on each side of the mask sample that could be used to reduce the effective area of the filter in the filter holder. The results for the flow curves (plotted together) are shown in Figure S10. Reasonable consistency between measurements with different filter areas is evident.

Section S4: Additional information and considerations to supplement main text

It is important to carefully outline a number of caveats and other considerations related to our measurement techniques and mask ranking system. These are simply meant to be an outline of general ideas that guided our thought process during the work.

Our setup measures two intrinsic properties of the filtration material of a face mask: its ability to filter aerosols and its flow impedance. We discuss considerations related to these properties as well as how they relate to the sealing ability in the following:

Filtration considerations

Real-time aerosol measurements are specifically used to provide concurrent feedback to users, and avoid filter sampling and weighing that would slow down the evaluation timescales and throughput. The bin pulse outputs of the AirNet were measured with pulse counters (HP 53131A Universal Counter) and tabulated manually, but this could easily be automated, as these outputs are also available through an ethernet connection. Outputs from the SEARCH monitors are fed into a cloud-based data plotting service (Grafana), from which real-time data for each test can be monitored, extracted, and analyzed.

An example of the comparative calculations between a circular sample of a mask in a filter holder and the full mask is as follows:

Face Velocity = Flow Rate (Q) / Surface Area (A)

$\text{Face Velocity}_{\text{Filter}}$ = 4.5 LPM /7.3 cm^2 = 10.3 cm/s

$\text{Face Velocity}_{\text{Mask}}$ = 105 LPM /170 cm^2 = 10.3 cm/s

Measurements of filtration efficiencies were made more robust by measuring across a series of dilution factors to gain multi-point measurements across a range of test aerosol concentrations at a given face velocity. This included measuring aerosol number concentrations while varying the source flow from the chamber, ranging from a "blank" containing a surplus of dilution air (i.e. overflow into the source chamber) to several aerosol concentrations well above any background signal. Measurements at each of these dilution conditions were made both with and without a mask in place (Figure S6). This allows a number of potential instrumental artifacts to be identified: (a) non-linearity in the downstream detector at high concentrations, (b) small leaks in the system that could result in a shift of the expected flow rate from the source chamber, and (c) a non-zero background in counts arising either from the instrument or from aerosols in the house air feeding the system. This multi-point approach was viewed as more robust than single point measurements in general, and was employed to generate the primary results shown in Figure 4 below, where the ratios between the slopes for the mask and no-mask dilution curves were used to derive the filtration efficiencies for each aerosol size bin.

Filtration Efficiency [%] = $(1- \text{Slope}_{\text{mask}}/\text{Slope}_{\text{no mask}}) \times 100\%$

where slope is in units of (#/m^3) / LPM.

Checks were performed to ensure that reasonable results could be obtained using single concentration measurements (i.e. one specific Q_{source} setting) as long as one is careful to check the issues outlined above periodically.

The downstream aerosol particle counters in this setup measure the number of particles that pass through a filter per unit volume of air in a specified aerosol-size bin, for a given total volume flow rate (e.g. 4.5 SLPM) through the filter. The volume flow rate divided by the circular filter opening area (d = 3.05 cm, area = 7.3 cm^2) yields a face velocity (cm/s). The aerosol count is plotted as a function of the dilution factor (DF) of aerosols from the source chamber, which is defined as the flow from the source divided by the total flow through the filter. The counts are generally linear with dilution and the results are fit with a straight line whose slope is determined.

These slopes, across four aerosol size bins, are measured with a filter in place and with no filter in place (what we refer to as a "blank") and we obtain a penetration ratio by taking the ratio of the two slopes. In practice, since we are measuring these ratios for the same total volume flow rate, we simply plot the counts versus volume flow from the source chamber, but the ratio of slopes is the same. The "filtration efficiency" of a material is then is defined as 100* (1 – penetration ratio), and expressed in %. We think of this as an "intrinsic" measurement because we believe that a measurement of a filter with a different area would yield the same result as long as we matched the face velocities.

For a preliminary rank ordering of masks, we find that it is sufficient to use one volume flow rate to characterize all the mask materials, as shown in Figure 4. However, it is important to recognize that the filtration efficiency is a function of the *face velocity*, as was illustrated in Figure 5. Generally, the filtration efficiency *decreases* with *increasing* face velocity for the smaller aerosols focused on here.

For a given mask, the face velocity will be the volume flow rate divided by the specific mask area. During the course of a human breath, the volume flow rate varies. Therefore, a mask is really experiencing a range of face velocities. For simplicity and consistency with regulation tests (1) we primarily use a face velocity of 10 cm/s, which corresponds to an inspiratory breathing volumetric flow rate of 105 LPM for the area of a "standard N95" mask (~170 cm^2) and provides a challenging face velocity to discern the filtration capabilities of masks.

In order for us to compare masks more directly, we would therefore want to measure the area of each mask, and tune our total volume flow rate to measure each mask at the face velocity corresponding to the standard breathing volume flow rate for that mask. Alternatively, using the dependence of the filtration efficiency on face velocity over an appropriate range for each material, and then fitting these results with a curve, we could correct the filtration efficiency of any mask by its area relative to the area of the standard N95 mask.

Impedance considerations

We measure the impedance of each mask material using a separate setup that uses a filter holder for samples of diameter 40mm as shown in Figure S2. The measurement of a pressure difference (mm H_2O) divided by a face velocity (cm/s) is an intrinsic impedance measurement that is independent of sample area, which we checked explicitly with one particular sample by modifying the filter holder to define various different filter areas.

As with the filtration measurements, the area of the mask plays an important role. However, that role is simpler to characterize. Our results were summarized by presenting the intrinsic impedance for each mask material and by defining the "breathability index" of a given mask relative to that of a standard N95. The actual pressure difference across the mask will be the assumed breathing volume flow velocity (for example, one might use the "standard breathing volume flow rate") multiplied by the intrinsic impedance divided by the mask area. Hence the "breathability index" should be corrected by the area ratio of the N95 mask to the specific mask as:

Corrected Breathability Index = Breathability Index * (Mask Area/ N95 Standard Area)

Purely from a breathability standpoint, there is likely a threshold above which a mask will feel very breathable, so this correction may not be very important as long as the mask is far enough above the threshold, as is the case for all that we measured. However, if a mask does not seal perfectly then the flow impedance could have an important role in the overall filtration, described in further detail below.

Interplay between flow impedance, filtration, and seal

A mask is evaluated for its ability to seal using a standard "fit testing" technique noted above and which is performed by Yale's Department of Environmental Health and Safety (2). Without trying to factor in accurate quantitative measurements of seal quality, we discuss here theoretical considerations related to our measurements of impedance and filtration. One consideration is that the seal against the face is rarely "perfect" (i.e. leak tight). A "leak" in the face seal is characterized by its own extrinsic impedance defined by the volume flow through the leak divided by the pressure difference across the mask (in mm H_2O/ cm^3/s). This flow path will be in parallel with flow going through the mask. We can think of the former as the "unfiltered flow path" and the latter as the "filtered flow path." We assume that the "unfiltered flow path" is not filtered at all; i.e. all aerosols can move through this leak.

Suppose two masks with the exact same filtration efficiency have different flow impedances (i.e. breathability). The one with higher flow impedance through the mask material (as measured in this study) will have a greater potential for "unfiltered" flow around the edges. Therefore, if given equal aerosol filtration efficiencies, a mask with higher breathability should be preferred over one with lower breathability. Practically, we factor this into our pipeline using the intrinsic breathability values, with a more detailed consideration amongst the top candidates, such as how each mask actually seals.

Section S5: Additional details on the quick assessment method

We want to emphasize that the quick assessment method (Figs. 3, S12) shows promise to be a viable, relatively low cost alternative to more sophisticated techniques, while maintaining adequate accuracy and reproducibility for ranking mask filtration efficiency. Comparison of the results with our full technique in Fig. 7 is essentially a validation of its usefulness. To make the point a little more clearly, Fig. S11 shows raw data obtained from an AirNet 210, for different masks successively installed in the filter holder alternated with blank runs with no filters in the holder. The AirNet we used for the rapid method could only output signals in two of the size bins, so we worked with the 0.2 - 0.3 um and 0.3 - 0.5 um bins (other models should have access to all 4 bins). These analog outputs, converted to a voltage with a resistor, were read by a "teensy" microprocessor and output to a serial monitor using Arduino IDE software. The voltage readings were converted to particle counts with a simple calibration procedure. The raw data shown are simply a plot of these two bin counts versus time for the array of samples, run in two consecutive segments.

Plotting the raw data on a log scale (which necessarily means that data for counts of zero are not visible) allows an almost immediate ranking of samples and simple determination of samples that are poor filters relative to an N95. The distance on a log scale between the blank counts and the filter counts directly measures the penetration ratio for a sample. For example, it may be noted directly from Fig. S11 that Masks 3, 22, and 23 are all extremely poor, while Masks 2, 16, and 19 are very close to parity with an N95 (sample 0), which are in turn followed closely by Masks 5, 9, 13, 18 in quality. These filtration efficiencies, while not exactly the same as those determined from the full setup, are reasonably close and rank similarly.

Key to making this simple technique useful, is the ability to tune the face velocity to be in a range that is relevant to typical breathing values in a mask, as was discussed at length in the main body of the paper. We used acrylic laser-cut rings to do this (for this method, we worked at a face velocity of ~15 cm/s), and took advantage of the AirNet capacity for maintaining a constant flow rate using a critical orifice. This point should be kept in mind should another detector be tried in this type of arrangement.

One pitfall of the technique that is evident from running replicate samples on different days, is that slight differences in absolute results for penetration ratios are observed, presumably because the size distribution, chemical composition, and concentrations of aerosols in the room are not reproducibly controlled as in the full setup. Although there are ways to reliably cross-calibrate data taken under different conditions, a practical solution to this issue is simply to run a standard set of samples (both good and poor) that span a reasonable range of penetration ratio (as well as the benchmark N95) along with any new samples being measured. With that, comparative rankings from different data runs (on different days, with different aerosol populations) may be obtained.

Supplemental Figures and Tables

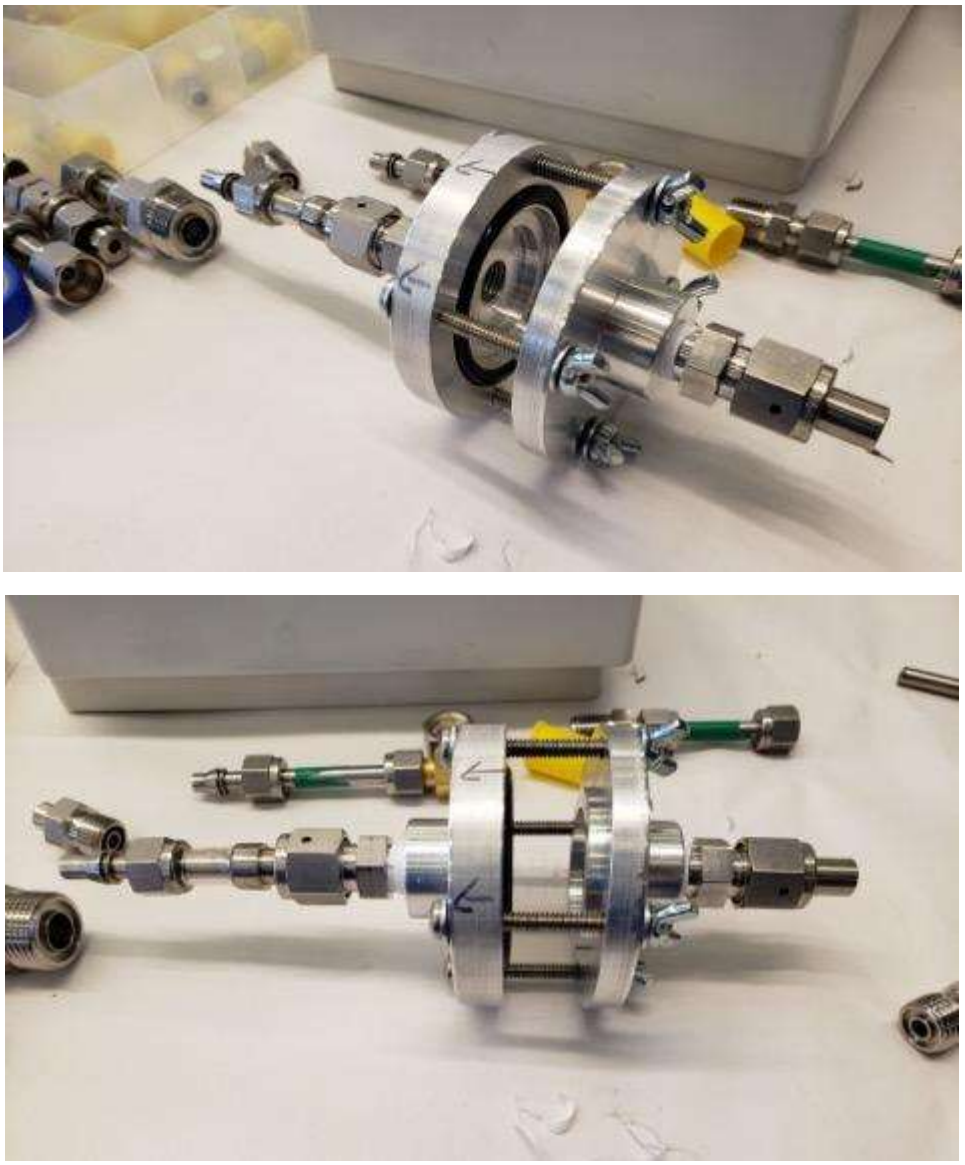

Figure S1: Final design for the metal filter holder, machined to securely hold a disk of filter material for testing. The o-ring shown clearly in the top panel creates an air-tight seal around the material to reduce leaks into the sampling system. A set of four bolts with corresponding wing nuts allow for easy access into the filter holder to change out material while providing a secure clamp around the material. The resulting area of the mask material exposed to flow in this setup was 30.5 mm.

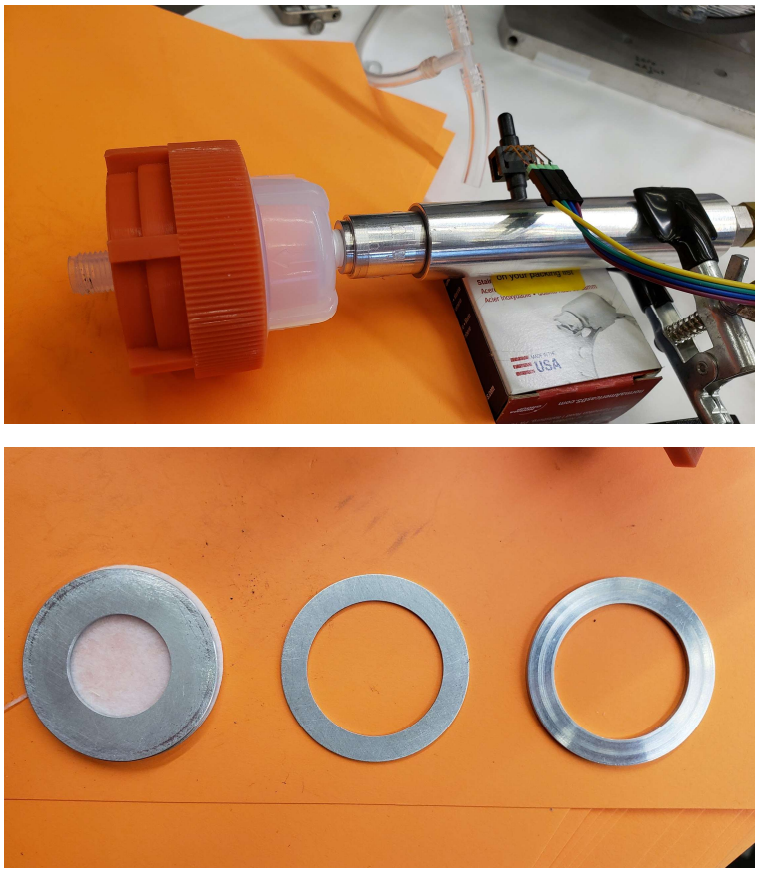

Figure S2: Example of the Teflon filter holder and metal rings used to seal a disk of mask material and modify the face velocity, used in both the flow impedance testing (Figure 2) and rapid screening setup (Figure 3).

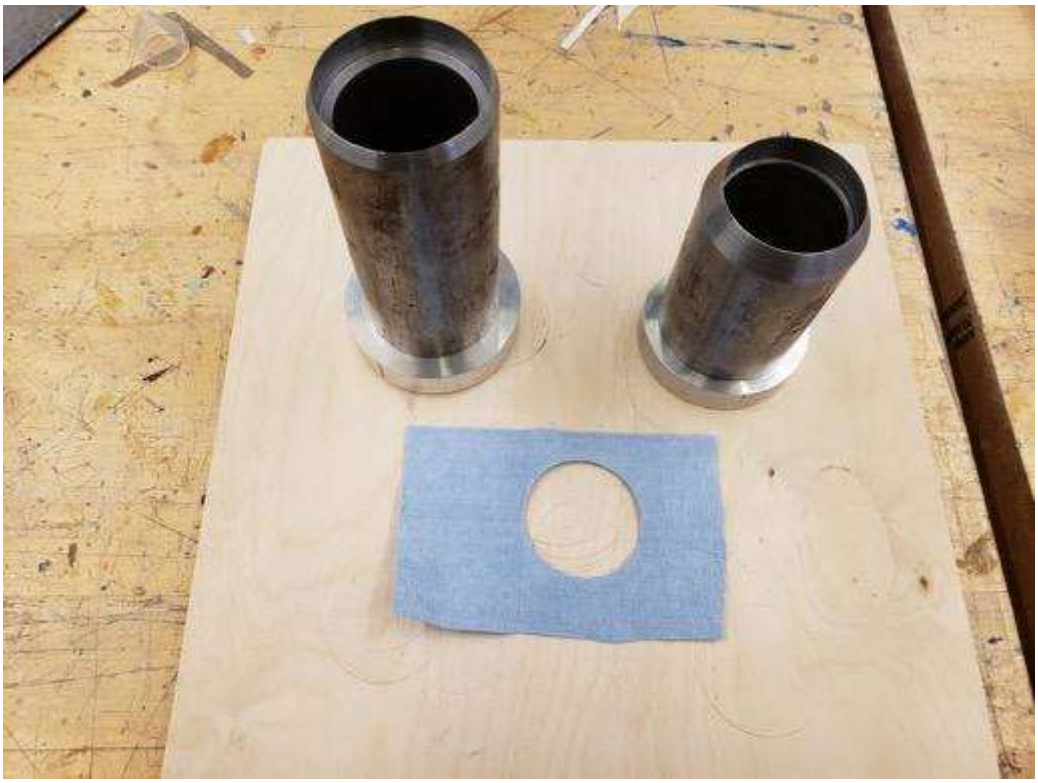

Figure S3: Dies were machined at specific diameters to cut mask filter material samples at consistent sizes. In the most recent round of mask filtration testing, the die cut out disks 30.5 mm in diameter.

Figure S4: Example of circular cutouts of a consistent known area are used to evaluate the filtration efficiency of each alternative mask. Data from each test is analyzed in terms of total mass area, scaled up from the circular disks.

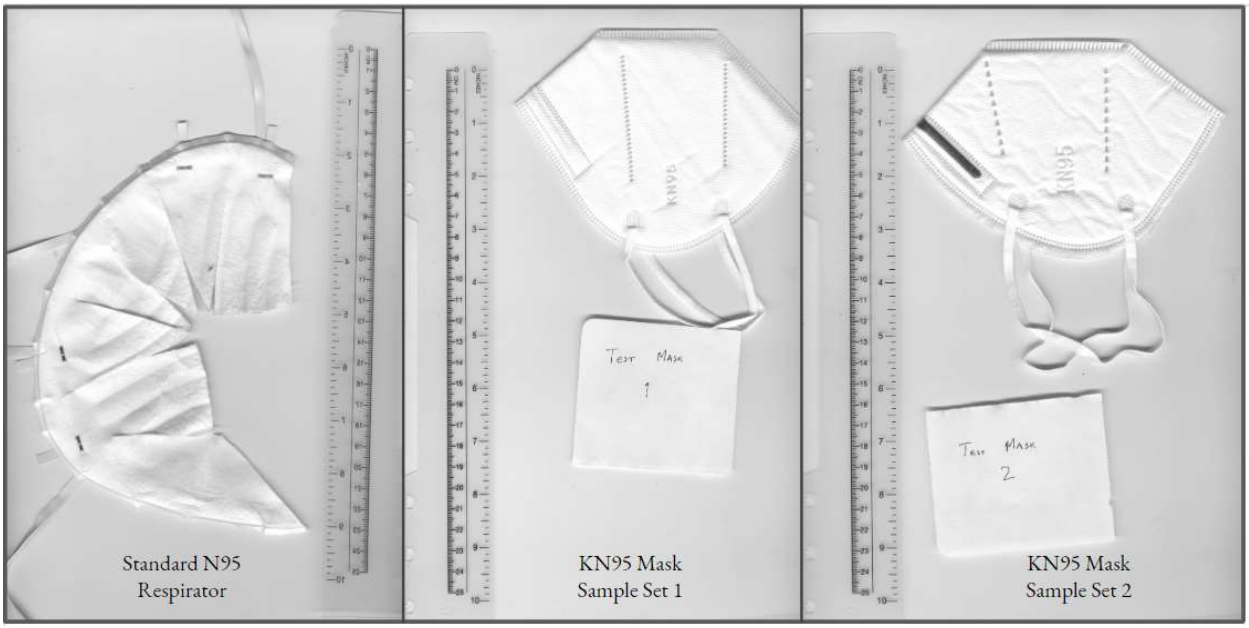

Figure S5: Techniques for determining areas of N95-like masks. An image of the mask, along with a ruler for scale, is loaded into ImageJ, an open source, image processing and analysis software. The image scale is calibrated using the markings on the ruler. The masks typically have a seam slightly inside the edge of the mask, where the filter materials are joined; this seam is assumed to be where the mask seals to the user's face. Areas are always measured from just inside this seam. Most of the masks simply lie flat on their side, and are symmetric, and so the total area is generally two times the area of one side. This area is determined using ImageJ's measurement tools, and then multiplied by two to get the total area. For masks that are not symmetric, but still fold flat, the total area can be found by summing the areas of both sides, found with ImageJ's measurement tool. Masks that do not lie flat are cut so that they lie flat, and are then measured.

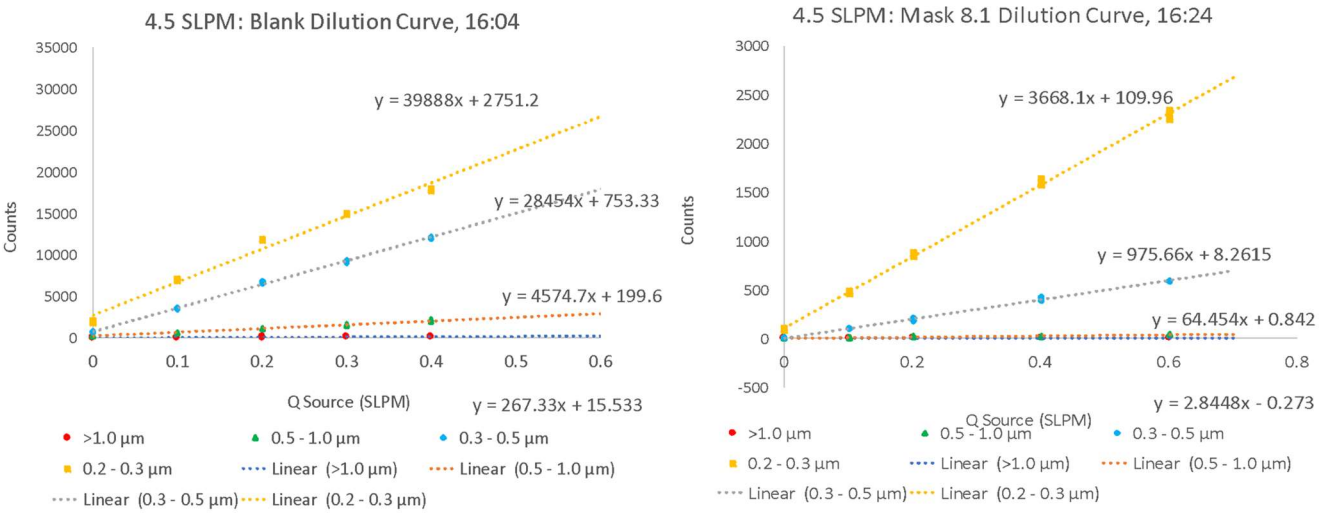

Figure S6: Multi-point derivations of aerosol filtration efficiency at multiple test aerosol concentrations (described in filtration methods section), shown here for one mask sample tested at 4.5 SLPM (i.e. 10 cm/s). The "blank" test (left) is without a mask in place and the figure on the right is with a mask sample in place.

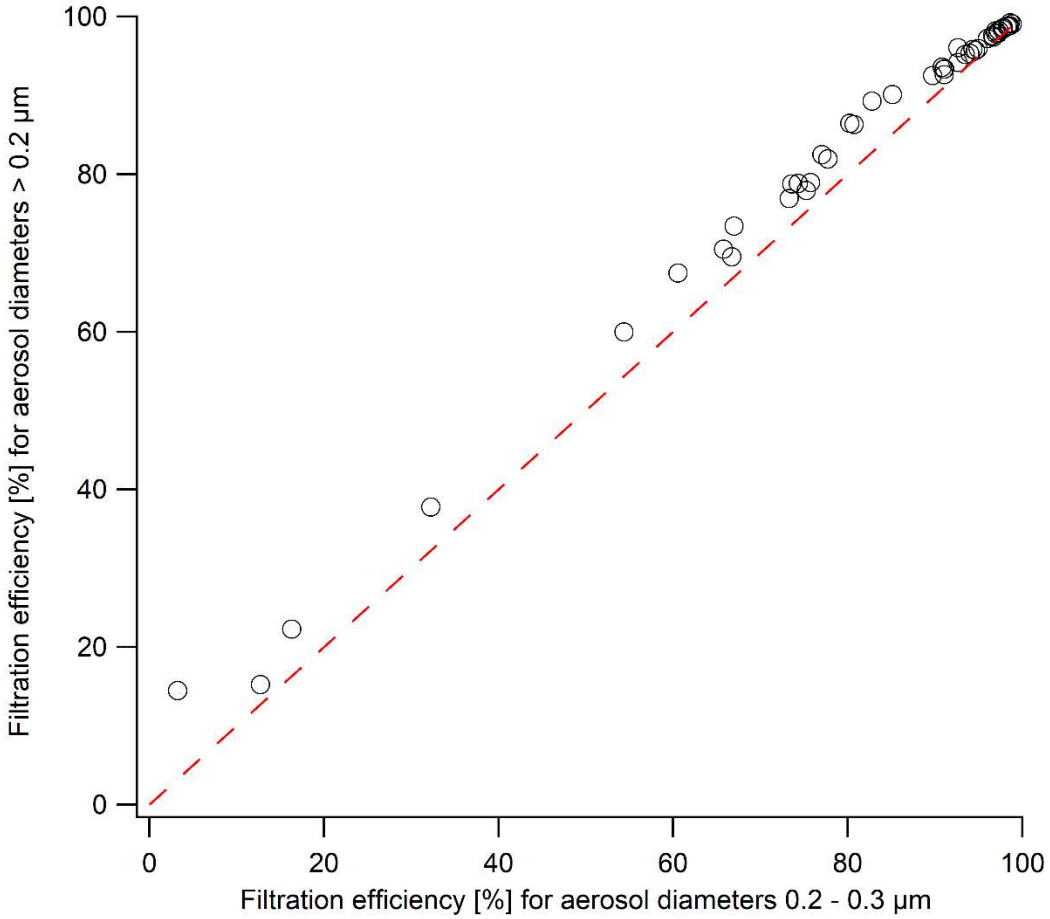

Figure S7: Comparison of filtration efficiencies for 0.2 µm and higher and 0.2-0.3 µm size range (efficiencies are both calculated as a function of aerosol number concentrations). Results are similar and slightly higher for all aerosol sizes larger than 0.2 µm given that larger aerosols are filtered more effectively. Calculation based on all particle sizes is more similar to NIOSH calculations of mass concentration-based efficiencies, while focusing on the solely on the 0.2-0.3 µm size bin is more similar to the FDA method that looks solely at filtration of 0.1 µm latex spheres (1).

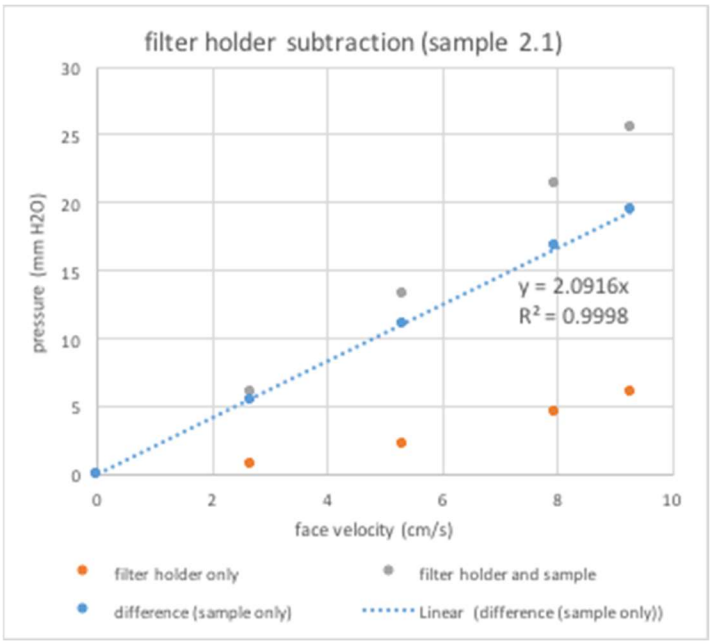

Figure S8: Flow impedance subtraction to eliminate impedance of filter holder (see discussion in method section)

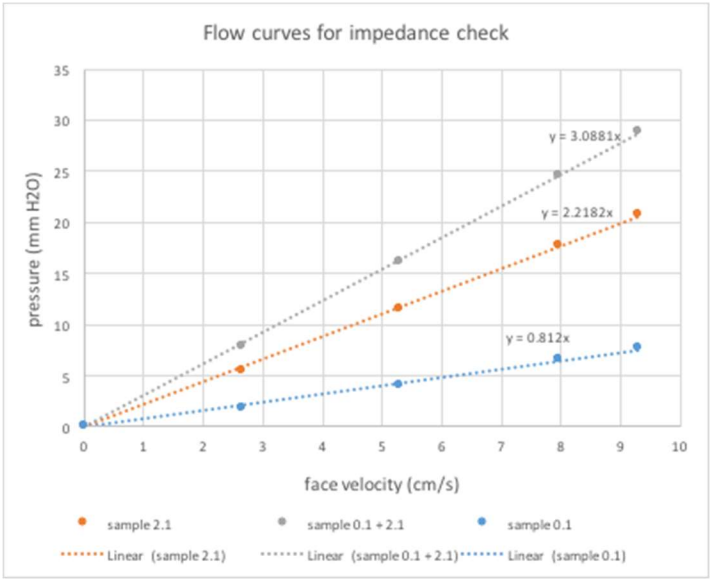

Figure S9: Flow impedance for 2 filters and then with both filters stacked in series

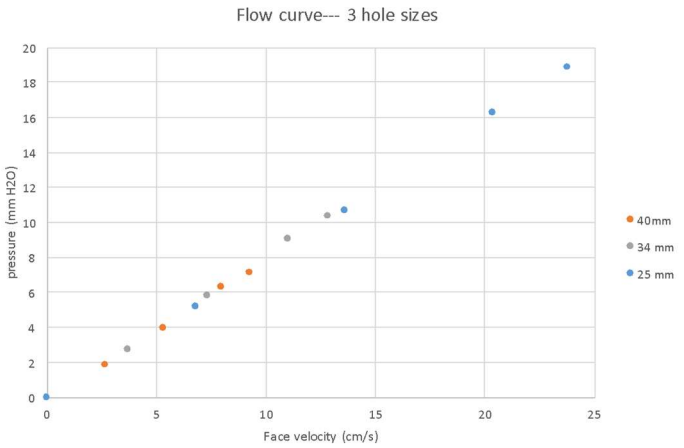

Figure S10. Pressure vs. face velocity curve for 3 different areas of same filter material.

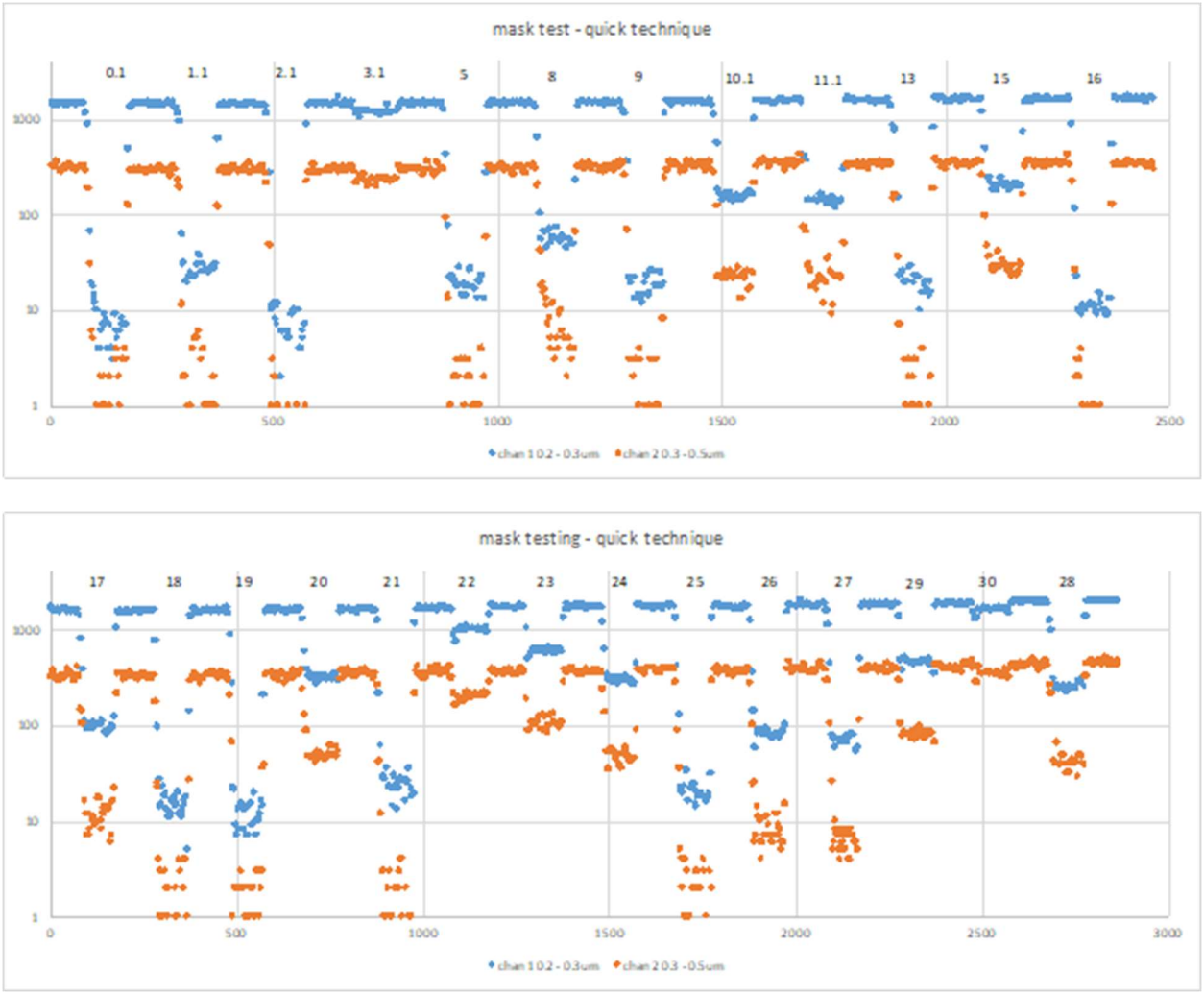

Figure S11: Rapid screening technique where 26 masks are profiled in 80 minutes. Shown here at 14.8 cm/s on a log scale for aerosol number concentrations on the y-axis (units: are # / 230mL).

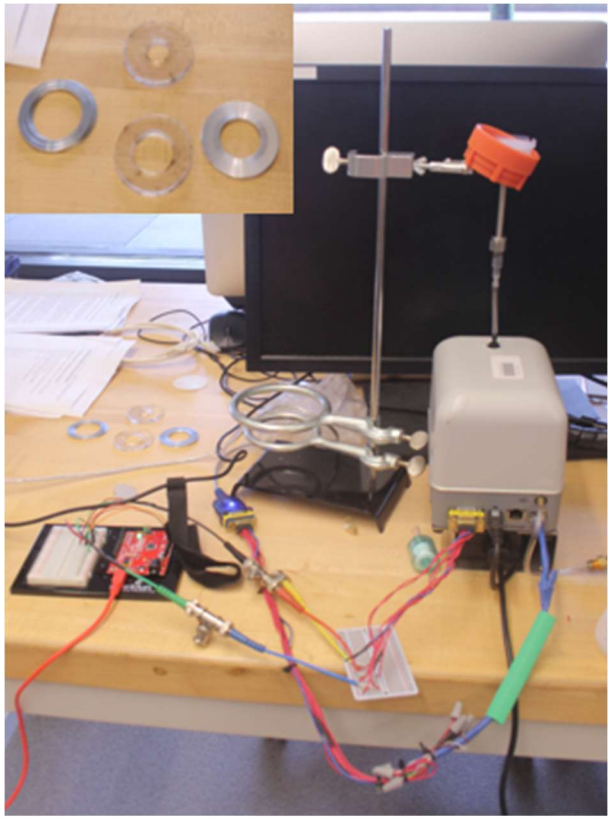

Figure S12: Quick assessment apparatus. Filter holder (orange) connected directly to AirNet, whose analog outputs are interfaced to a computer via Arduino or Teensy. Inset at top shows rings used for impedance checks as well as to adjust face velocity for filtration measurements.

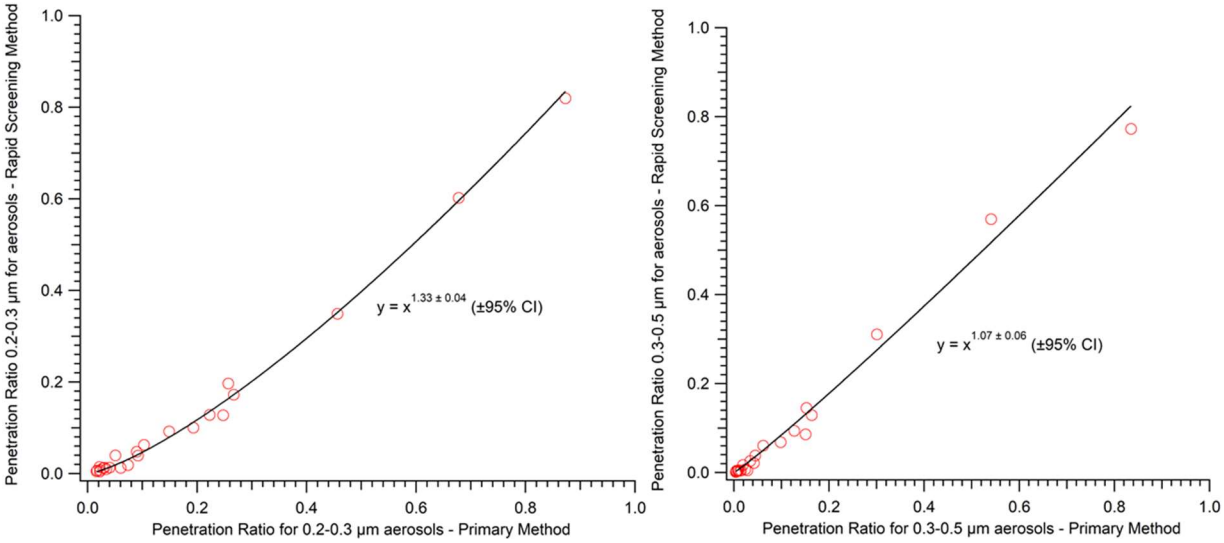

Figure S13: Power function fits (with 95% confidence intervals) for the rapid screening approach vs. the primary method for penetration ratio (i.e. 1 - filtration eff./100) shown for aerosols of 0.2 - 0.3 µm (left) and 0.3 - 0.5 µm (right). The results demonstrate good correlation between the two approaches. These differences in filtration efficiencies (and thus penetration ratios) are potentially due to the combined effect of differences in in-room aerosol size distributions and face velocities (10 cm/s vs. 14.8 cm/s for the primary vs. rapid approach). The proportion of smaller particles in the in-room rapid screening tests suggests that the particle number distributions in the room were shifted to smaller sizes relative to the incense, which has a greater proportion of larger particles in the 0.2-0.3 µm bin.

Table S1: Summary of mask testing results for filtration and breathability

ID #	Mask Type	Intrinsic Impedance (mm H_2O/(cm/s))	Area (cm^2)	Extrinsic Impedance (mm H_2O)/(cm^3/s)	Filtration Efficiency for Particle Size Bins			
					>0.2 µm (total)	0.5 - 1 µm	0.3 - 0.5 µm	0.2 - 0.3 µm
0	Regulation N95	0.81	168	0.0048	98.5	99.9	99.4	97.7
1	Labeled "KN95"	0.98	204	0.0048	96	98.4	97.6	92.6
2	Labeled "KN95"	2.09	187	0.0112	98.8	100	99.6	98.2
3	Commercial Alternative Surgical Mask	0.41	-	-	15.2	23.9	16.5	12.7
5	Labeled "KN90"	1.23	-	-	98.2	99.6	99	96.9
6	Donated homemade mask	1.34	-	-	14.5	27.2	16.0	3.2
7	Labeled "KN90"	0.85	-	-	89.2	97.2	93.1	82.7
8	Labeled "KN95"	0.76	-	-	93.5	98.5	96.5	90.8
9	Labeled "N95"	0.95	-	-	95.3	98.6	97.1	93.9
10	Labeled "KN95"	1.81	-	-	86.3	96.2	90.1	80.6
12	Labeled "N95"	1.28	198	0.0065	98.2	99.7	99.1	97.2
13	Labeled "N95"	0.54	225	0.0024	97.2	98.7	98.5	95.9
15	Labeled "KN95"	0.41	-	-	77.9	92.3	84.9	75.2
16	Labeled "KN95"	1.75	205	0.0085	98.7	99.6	99.5	98.2
17	Labeled "KN95"	1.07	221	0.0048	92.5	98.3	95.5	89.7
18	Labeled "N95"	0.91	221	0.0041	97.5	99.7	98.7	96.5
19	Labeled "N95"	0.96	-	-	98.3	99.9	99.1	97.7
20	Unlabeled Surgical Mask	0.69	-	-	78.8	88.5	84.7	74.3

21	Labeled "S-KN95"	1.26	199	0.0063	98.5	100	99.5	97.8
22	Labeled "S-KN95C"	0.32	-	-	37.7	57.3	45.9	32.2
23	Labeled "KN95"	0.51	-	-	59.9	74.1	69.9	54.3
24	Labeled "KN95"	1.1	-	-	76.9	90.1	83.6	73.2
25	Labeled "KN95"	1.24	215	0.0058	97.8	99.9	99.2	97.1
26	Labeled "N95"	1.26	206	0.0061	92.6	98.4	95.7	91
27	Labeled "KN95"	0.89	224	0.004	95.9	98.4	98.1	94.9
28	Unlabeled Surgical Mask	0.75	-	-	81.9	93	87.3	77.7
31	Labeled "KN95"	1.01	-	-	98.8	99.9	99.3	98.4
32	Labeled "N95"	1.05	-	-	97.9	99.7	98.7	97.1
33	Labeled "KN95"	0.86	-	-	70.4	83.4	74.8	65.7
34	Unlabeled Surgical Mask	0.57	-	-	78.7	90.3	83.9	73.5
35	Labeled "KN95"	1.51	-	-	95.8	99.3	97.5	94.3
36	Labeled "KN95"	1.05	-	-	97.8	99.9	99.1	96.9
37	Labeled "KN95"	1.07	-	-	94.1	98.6	97	92.5
38	Labeled "KN95"	1.01	-	-	93.3	99.2	97.3	90.9
39	Labeled "KN95"	0.65	-	-	95.6	98.9	97.8	94.6
40	Labeled "N95"	1.02	-	-	98.8	100	99.4	98.5
41	Unlabeled Surgical Mask	0.37	-	-	78.9	95.5	85.4	75.7
42	Unlabeled Surgical Mask	0.53	-	-	82.4	92.3	87.6	77
43	Labeled "KN95"	1.36	-	-	99	99.6	99.6	98.8

44	Labeled "KN95"	1.48	-	-	97.4	99.6	99	96.6
45	Unlabeled Surgical Mask	0.71	-	-	69.5	82.5	75.9	66.7
46	Unlabeled Surgical Mask	0.71	-	-	67.4	81.6	74.7	60.5
47	Unlabeled Surgical Mask	0.63	-	-	22.3	35.5	28.6	16.3
48	Unlabeled Surgical Mask	0.69	-	-	73.4	87.0	80.8	67.0
49	Unlabeled Surgical Mask	0.43	-	-	95.2	98.7	97.3	93.4
50	Labeled "KN95"	1.17	-	-	93.4	98.6	96.1	91.1

Notes:

- Areas were not measured for all masks (as discussed in text).
- Mask numbering here is referring to the internal logging, not the rank-ordered performance shown in Figure 4.